J. Micromech. Microeng. **17** (2007) 1275–1280 doi:10.1088/0960-1317/17/7/009

# A novel CMOS out-of-plane accelerometer with fully differential gap-closing capacitance sensing electrodes

**Chuanwei Wang**[1], **Ming-Han Tsai**[2], **Chih-Ming Sun**[2] **and Weileun Fang**[1,2]

[1] Department of Power Mechanical Engineering, National Tsing Hua University, Hsinchu, Taiwan
[2] Institute of Microelectromechanical System, National Tsing Hua University, Hsinchu, Taiwan

E-mail: fang@pme.nthu.edu.tw

Received 11 April 2007, in final form 10 May 2007
Published 5 June 2007
Online at stacks.iop.org/JMM/17/1275

**Abstract**
This study presents a novel CMOS-MEMS out-of-plane linear accelerometer. This capacitance-type accelerometer contains specially designed gap-closing sensing electrode arrays with on-chip fully differential sensing circuits. Moreover, the comb-finger electrodes have the characteristics of the high fill factor and sub-micron gap to increase the sensing capacitance. Thus, the sensitivity and signal-to-noise ratio can be further improved. This study has established a post-CMOS wet-etching process to realize the accelerometer with sensing electrodes of the sub-micron gap in the out-of-plane direction. The present accelerometer has been demonstrated using the standard TSMC 2P4M process plus the post-release technique. The measurement results demonstrate that the accelerometer has a sensitivity of 1.14 mV $g^{-1}$, and a nonlinearity of 3.4%.

(Some figures in this article are in colour only in the electronic version)

## 1. Introduction

The linear accelerometer has been extensively applied in the automobile industry. Presently, the accelerometer finds even more applications in consumer electronics, for instance, the cell phone, PDA, digital still camera (DSC), laptops and video games. The requirement of the multi-axes accelerometer is also significantly increased. Thus, in addition to cost, the size of the accelerometer becomes an important design consideration. To monolithically integrate a three-axis accelerometer on a single chip is an effective approach to reduce not only the size but also the cost. However, there are very few available monolithic integrated three-axis accelerometers [1–3]. In [1], a monolithic three-axis micro-g accelerometer has been realized using the integration of surface and bulk micromachining processes. In [2], a monolithic three-axis accelerometer has been realized using the integration of surface micromachined mechanical structures and the CMOS IC. The three-axis spring-mass dynamic systems have been monolithically implemented on the SOI wafer in [3]. However, the sensing circuits are integrated to the SOI chip using the bonding technology.

The standard CMOS process has been extensively applied to fabricate MEMS devices. The major advantage of the CMOS process is the monolithic integration of the IC and MEMS components. This characteristic is especially important for the sensor applications, such as the accelerometer, microphone, etc. Moreover, the stable foundry service is ready for the CMOS process. Presently, there are various CMOS-MEMS in-plane accelerometers presented in [4–6]. However, there are less CMOS-MEMS out-of-plane accelerometers reported in [7–9]. Due to the fixed materials of stacking layers and the post-process, the existing out-of-plane capacitive sensing electrodes in [7, 8] behaved as parallel vertical combs. Thus, the total sensing area of each comb electrode is limited to the thickness of metal layers, and the sensing gap is restricted by the RIE (reactive ion etching) process.

  

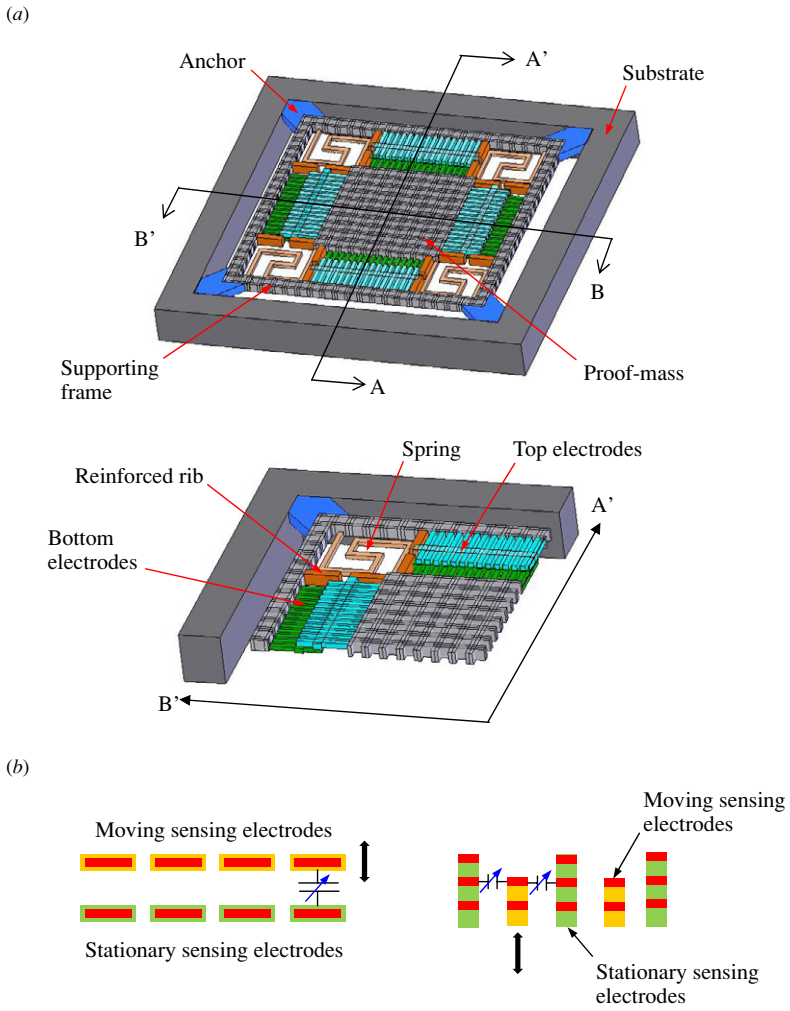


**Figure 1.** The schematic illustrations of (*a*) the present CMOS out-of-plane linear accelerometer, and (*b*) comparison of the present gap-closing sensing electrodes and the existing parallel vertical comb sensing electrodes.

In this study, the development of a novel CMOS out-of-plane ($z$-axis) linear accelerometer is reported. The gap-closing capacitance sensing technique is employed in the present CMOS out-of-plane accelerometer. A post-CMOS process is exploited to realize the capacitance sensing electrodes of a sub-micron gap. Hence, this accelerometer enables sensing electrodes with the characteristics of a high fill factor and sub-micron gap to increase the sensing capacitance. In addition, the design of the sensing electrode arrays enables the implementation of fully differential sensing circuits. Thus, the sensitivity and signal-to-noise ratio can be further improved. The present accelerometer has been demonstrated using the standard TSMC 2P4M process plus the post-release technique. The present processes are easy to integrate with those for in-plane accelerometers in [10], so as to further implement a monolithic three-axis CMOS accelerometer.

## 2. Design concept

The present out-of-plane linear accelerometer employs novel fully differential capacitive sensing electrodes of sub-micron gap design, and further implements the design using a novel post-CMOS process. As shown in figure 1(*a*), the present accelerometer consists of a proof mass, four flexible springs, a supporting frame, four stiff suspensions and four pairs of comb-finger sensing electrode arrays. The supporting frame is anchored to the substrate using four stiff suspensions, and acts as a stationary component of the accelerometer. The proof mass is connected to the supporting frame using four flexible springs, and acts as a movable component of the accelerometer. The sensing electrodes attached to the proof mass and the supporting frame act as the moving and stationary electrodes, respectively. The proof mass is subjected to an out-of-plane inertia force when an external out-of-plane acceleration is applied on the accelerometer. Thus, the spring-mass system will experience a displacement in the out-of-plane direction, so as to change the gap between the moving and stationary electrodes, as indicated in the left-hand illustration of figure 1(*b*). The displacement as well as the external acceleration can be detected by the capacitance change of the electrodes. As a comparison, the right-hand illustration shows the existing vertical comb-electrode out-of-plane accelerometer [8].

To improve the sensitivity of the accelerometer, the proof mass is designed to contain all of the four metal layers to

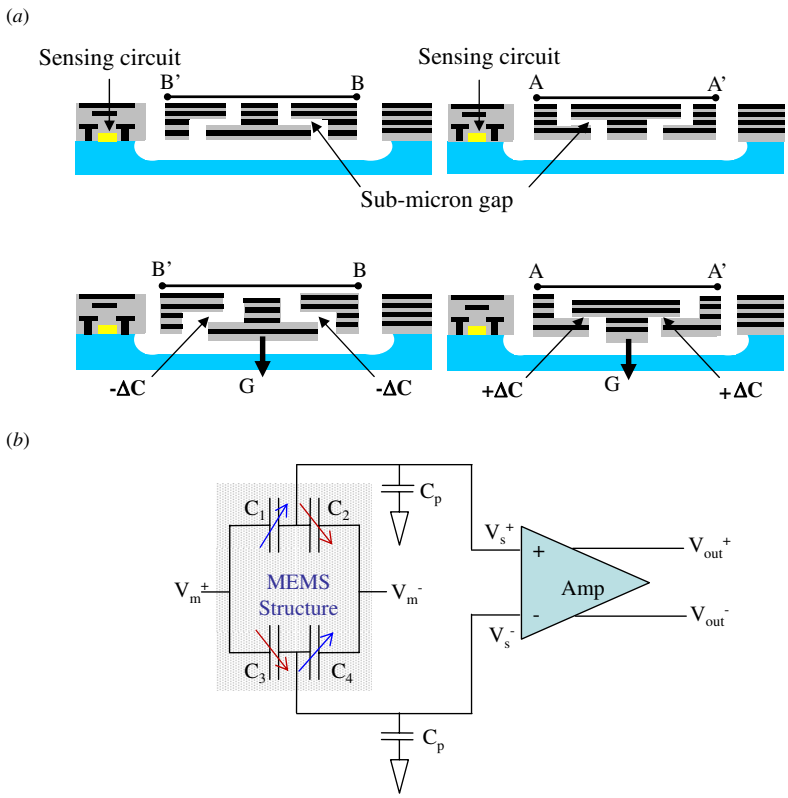


**Figure 2.** (*a*) The design concept of fully differential gap-closing sensing electrodes with capacitance changes of $+\Delta C$ and $-\Delta C$ at an acceleration $G$, and (*b*) the equivalent fully differential sensing circuit.

increase its inertia. In addition, the spring is designed to contain only two metal layers (metal-1 and metal-2 layers) to decrease its stiffness. The serpentine spring design is also used to reduce its out-of-plane stiffness and to further increase the sensitivity of the accelerometer. Nevertheless, the spring is much stiffer in the in-plane directions. The springs are placed at the corners of the proof mass to suppress the bending resulted from a thin-film residual stress. In addition, the supporting frame is exploited to match the bending of proof mass due to the residual stress [11]. Thus, the influence of the thin-film residual stress on the gap of sensing electrodes can be reduced. The supporting frame is also consisted of four metal layers to increase its stiffness. To ensure the supporting frame as a stationary structure, the stiffness of its suspensions is four orders of magnitude larger than that of the flexible springs. Moreover, there are three critical design considerations as follows.

### *2.1. Out-of-plane gap-closing electrodes of the sub-micron gap*

As illustrated on the left-hand side of figure 1(*b*), the accelerometer employs the gap-closing sensing electrodes in the out-of-plane direction. In addition, the sensing area is increased due to the high fill factor of the electrodes. As a result, the sensitivity of the present accelerometer can be improved. In addition, the present accelerometer contains a sub-micron gap between the moving and stationary comb fingers. This sub-micron gap is mainly determined by the thickness (0.65 $\mu$m) of the metal film using a post-CMOS wet-etching process. The process will be detailed in section 3. The sub-micron space allows an excitation of 160$G$, since the spring-mass design of this study gives an out-of-plane displacement of 4 nm/$G$. The gap between moving and stationary electrodes can also be tuned by etching more metal and dielectric layers.

### *2.2. Fully differential sensing electrodes*

Figure 2(*a*) shows the schematic illustrations of the $AA'$ and $BB'$ cross sections indicated in figure 1(*a*). In the $AA'$ cross section, the moving comb-finger arrays are designed to locate above the stationary comb fingers, whereas the moving comb-finger arrays in the $BB'$ cross section are placed below the stationary electrode arrays. As the proof mass is subjected to an acceleration $G$ in the downward direction, the moving comb fingers for both $AA'$ and $BB'$ cross sections will have a downward displacement. Thus, as indicated in the $BB'$ cross section, the gap between sensing electrodes is increased, and leads to a capacitance change of $-\Delta C$. Meanwhile, as indicated in the $AA'$ cross section, the gap between sensing electrodes is decreased, and experiences a capacitance change of $+\Delta C$. As a result, the sensing finger arrays designed in this study form a fully differential type sensing circuits to improve the sensitivity and signal-to-noise ratio, as shown in figure 2(*b*). The interface-integrated circuits which are monolithically built together with the accelerometer include a two-stage pre-amplifier and bias circuit. The pre-amplifier can provide totally 30 dB gain to increase the level of sensing

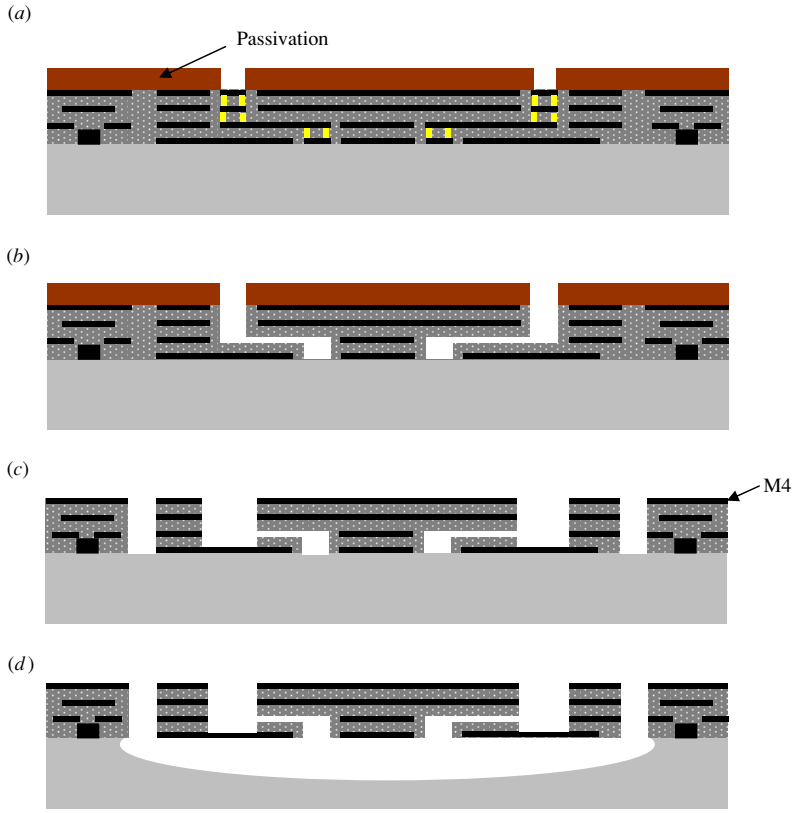


**Figure 3.** The fabrication process steps: (*a*) after the TSMC 0.35 $\mu$m 2P4M CMOS process, (*b*) metal wet etching for a sub-micron gap, (*c*) remove silicon oxide by RIE, and (*d*) release structure by $XeF_2$ isotropic etching.

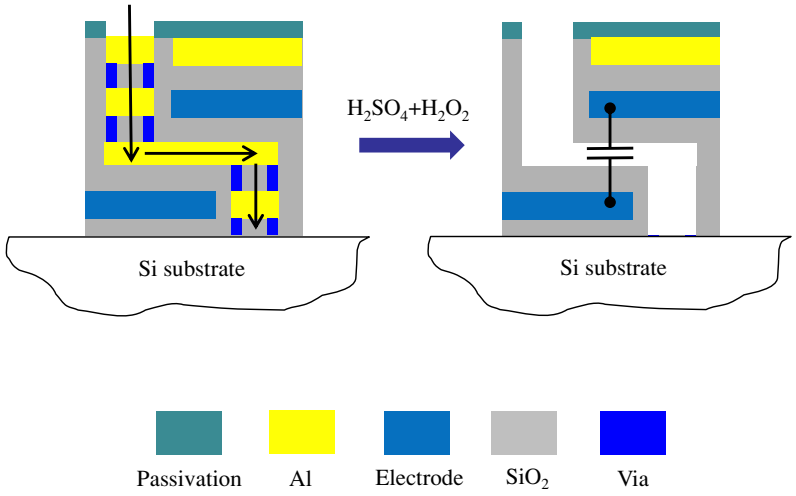


**Figure 4.** The details of metal wet etching to form the sub-micron gap.

signal. The bias circuit needs a 15 kΩ off-chip resistor and works with a 5 V working voltage. From the simulated result, the bandwidth of the pre-amplifier is 10 MHz and the parasitic capacitance is 150 fF.

## 3. Fabrication process flow

Figure 3 shows the process flow to realize the present accelerometer. The accelerometer was first fabricated using the TSMC 0.35 $\mu$m 2P4M CMOS process, as illustrated in figure 3(*a*). After that, the post-CMOS processes shown in figures 3(*b*)–(*d*) were employed to implement the suspended CMOS-MEMS accelerometer. As shown in figure 3(*b*), the $H_2SO_4$ and $H_2O_2$ solutions were used to etch through the metal and tungsten-via layers to form the sub-micron gap between the electrodes. Figure 4 shows more detailed information of figure 3(*b*), and the arrows indicate the paths of chemical etching. The passivation and dielectric film acted as the protection layer during chemical etching. The metal-4 aluminum film with no passivation layer was etched away

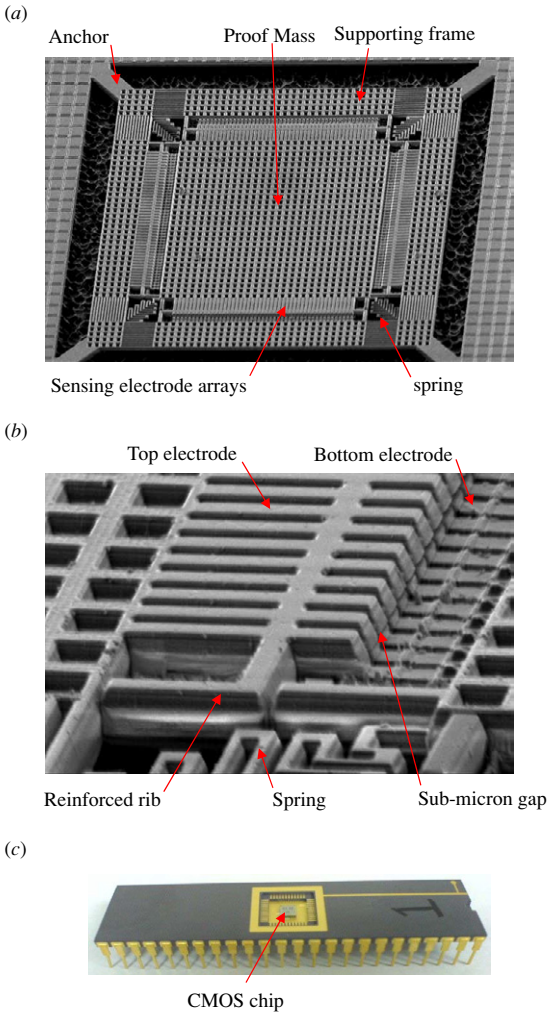


**Figure 5.** (*a*) The SEM micrograph image of a typical fabricated accelerometer, (*b*) the zoom-in SEM micrograph image of the accelerometer, showing the sensing electrodes with the sub-micron gap, and (*c*) the photo of a packaged accelerometer.

first, and then the tungsten vias were also attacked. After the vias had been etched through by chemical solutions, the metal-3 aluminum was attacked isotropically. Although the dielectric film acted as the etching stop layer, the $SiO_2$ layer surrounded by tungsten-via and metal-3 aluminum was able to be removed after these metal films were fully etched, as indicated in figure 4. On the other hand, the metal-3 and metal-1 aluminum layers protected by the $SiO_2$ film were survived after chemical etching, and acted as the top and bottom electrodes, respectively. In addition, the horizontal arrow in figure 4 indicates that the 0.65 $\mu$m thick metal-2 layer between the top and bottom electrodes was removed by chemical solutions. This etching process was exploited to define the sub-micron gap between the electrodes. Following the same concept, the metal-1 layer and the adjacent dielectric films were etched away, and the silicon substrate was exposed.

As shown in figure 3(*c*), the RIE (reactive ion etching) anisotropic etching was then employed to remove the passivation and dielectric films. In this process, the top metal layer (metal-4) acted as the etching mask to define the planar shape of proof mass, sensing electrodes and supporting

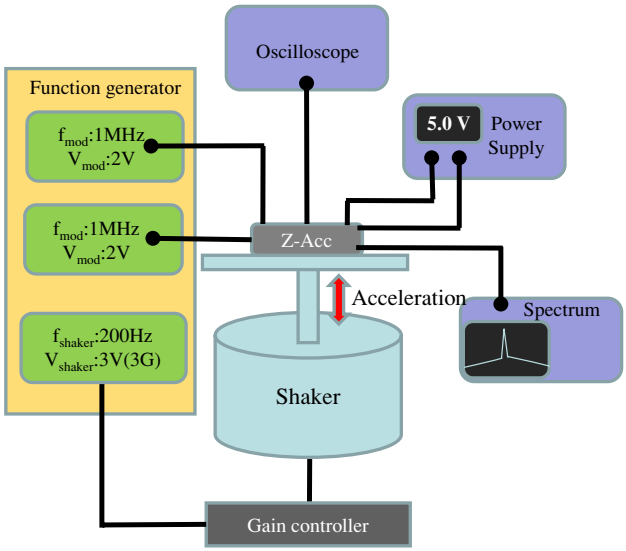


**Figure 6.** The test setup to characterize the accelerometer.

frame. However, the in-plane shape of springs was defined by the etching mask of the metal-2 layer during RIE. Thus, the thickness of springs was smaller than that of the proof mass and supporting frame, and the spring stiffness was also reduced [12]. The dielectric films between the top and bottom electrodes were not etched away after RIE to ensure the insulation of sensing electrodes. Finally, the substrate was etched isotropically using $XeF_2$ to fully suspend the components of the accelerometer, as illustrated in figure 3(*d*).

## 4. Experimental results

Figure 5 shows the SEM (scanning electron microscopy) photos of a typical fabricated accelerometer. The components of the accelerometer, such as the proof mass, sensing electrodes, springs and supporting frame, are clearly observed in figure 5(*a*). The corners of the supporting frame are anchored to the substrate by stiff plates, and the corners of the proof mass are also fixed to the supporting frame by springs. Thus, bending of the supporting frame and proof mass due to thin-film residual stresses are suppressed by the constraints at corners. The zoom-in SEM photo in figure 5(*b*) shows the top and the bottom sensing electrodes. In this particular case, the top and the bottom sensing electrodes represent the stationary and moving electrodes, respectively. The reinforced rib is exploited to prevent the sensing electrodes from bending by residual stress. The sub-micron gap between sensing electrodes can also be observed. In addition, the thickness difference between the spring and the proof mass is demonstrated in this photo. The packaged accelerometer is shown in figure 5(*c*).

This study established the measurement setup shown in figure 6 to characterize the performances of the accelerometer. During the test, the shaker and function generator were used to specify a base motion to excite the packaged accelerometer shown in figure 5(*c*). The dynamic characteristic of the shaker was monitored using a commercial accelerometer. Moreover, two function generators were also employed to provide modulation signals for fully differential sensing electrodes.

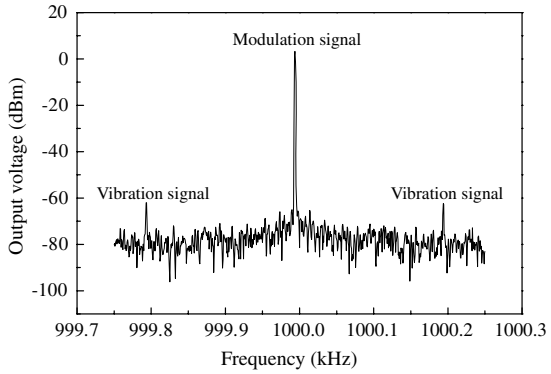


**Figure 7.** Spectrum of the accelerometer at an excitation of 200 Hz, 3 V (3*G*) using a shaker.

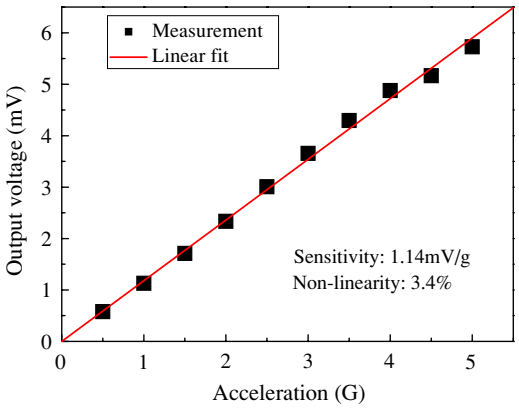


**Figure 8.** The variation of the measured output voltage with the input acceleration.

After that, the output voltage change from the accelerometer was characterized using the oscilloscope and spectrum analyzer. Figure 7 shows the results measured from the accelerometer after being driven by the shaker with a 3 V, and 200 Hz (i.e. 3*G*) harmonic (sinusoidal) excitation. The noise floor is 0.05 mV $Hz^{-1/2}$ with a modulation voltage of 2 V at 1 MHz. Figure 8 shows the output voltages of the accelerometer at different excitations by the shaker. It shows the output voltage increasing from 0.58 mV to 5.73 mV when the excitation increasing from 0.5*G* to 5*G*. As a result, the sensitivity of this integrated accelerometer is 1.14 mV $g^{-1}$ and the nonlinearity is 3.40%.

## 5. Conclusions

This study successfully designs and implements a novel CMOS capacitance-type linear accelerometer to detect the motion in the out-of-plane direction. The accelerometer contains the fully differential gap-closing capacitance sensing electrodes. Thus, the noise can be reduced. Moreover, a post-CMOS wet-etching process has been established to realize a sub-micron sensing gap between stationary and moving electrodes in the out-of-plane direction. Thus, the sensing capacitance can be significantly increased for a high fill factor of the sensing electrode and the sub-micron sensing gap. In application, the CMOS accelerometer has been demonstrated using the standard TSMC 2P4M process plus the post-release technique. The measurement results demonstrate that the present out-of-plane accelerometer has a sensitivity of 1.14 mV $g^{-1}$, and a nonlinearity of 3.40%. Since the present design is ready to integrate with the existing in-plane CMOS accelerometers, a monolithic three-axis CMOS accelerometer can be realized.

## Acknowledgments

This research was sponsored in part by Delta Electronics Inc and the National Science Council of Taiwan under grant of NSC-94-2212-E-007-026. The authors wish to thank the National Chip Implementation Center (CIC), Taiwan, for supporting the IC Manufacturing. The authors would also like to thank the Central Regional MEMS Research Center of National Science Council, Semiconductor Research Center of National Chiao Tung University and National Nano Device Laboratory of NSC for providing the fabrication facilities.

## References

[1] Chae J, Kulah H and Najafi K 2005 A monolithic three-axis micro-g micromachined silicon capacitive accelerometer *J. Microelecromech. Syst.* **14** 235–42

[2] Lemkin M and Boser B E 1999 A three-axis micromachined accelerometer with a CMOS position-sense interface and digital offset-trim electronics *IEEE J. Solid-State Circuits* **34** 456–68

[3] Matsumoto Y, Nishimura M, Matsuura M and Ishida M 1999 Three-axis SOI capacitive accelerometer with PLL C-V converter *Sensors Actuators* **A 75** 77–85

[4] Luo H, Zhang G, Carley L R and K Fedder G 2002 A post-CMOS micromachined lateral accelerometer *IEEE/ASME J. Microelecromech. Syst.* **11** 188–95

[5] Seidel H, Fritsch U, Gottinger R, Schalk J, Walter J and Ambaum K 1995 A piezoresistive silicon accelerometer with monolithically integrated CMOS-circuitry *Transducers'95 (Stockholm, Sweden, 25–29 June)* pp 597–600

[6] Sherman S J 1994 *Monolithic Accelerometer US Patent No.* 5345824S, Analog Devices, Inc.

[7] Xie H, Fedder G K, Pan Z and Frey W 2003 Design and fabrication of an integrated CMOS-MEMS 3-axis accelerometer *MSM'03 (San Francisco, CA, 23–27 February)* pp 292–5

[8] Lakdawala H and Fedder G K 2004 Temperature stabilization of CMOS capacitive accelerometer *IEEE/ASME J. Microelecromech. Syst.* **13** 559–66

[9] Boser B E and Howe R T 1996 Surface micromachined accelerometers *IEEE J. Solid-State Circuits* **31** 366–75

[10] Sun C M, Wang C, Wang C, Liu D H, -C Lu M S and Fang W 2006 A novel CMOS MEMS accelerometer with four sensing arrays *IEEE Sensors'06 (Daegu, Korea, 22–25 October.)* p 311

[11] Zhang G, Xie H, de Rosset L E and Fedder G K 1999 A lateral capacitive CMOS accelerometer with structural curl compensation *MEMS '99: 12th IEEE International Conference on Micro Electro Mechanical Systems (January 1999)* pp 606–11

[12] Xie H and Fedder G K 2000 A CMOS Z-axis capacitive accelerometer with comb-finger sensing *MEMS '00 (Miyazaki, Japan, 23–27 January)* pp 496–501